

1 Atmospheric $\Delta^{17}\text{O}(\text{NO}_3^-)$ reveals nocturnal chemistry dominates nitrate production 2 in Beijing haze

3 Pengzhen He¹, Zhouqing Xie^{1,2,3*}, Xiyuan Chi¹, Xiawei Yu¹, Shidong Fan¹, Hui Kang¹, Cheng Liu^{1,2,3}, Haicong Zhan¹

4 ¹Anhui Province Key Laboratory of Polar Environment and Global Change, School of Earth and Space Sciences, University
5 of Science and Technology of China, Hefei, Anhui 230026, China.

6 ²Center for Excellence in Urban Atmospheric Environment, Institute of Urban Environment, Chinese Academy of Sciences,
7 Xiamen, Fujian 361021, China.

8 ³Key Lab of Environmental Optics and Technology, Anhui Institute of Optics and Fine Mechanics, Chinese Academy of
9 Sciences, Hefei, Anhui 230031, China.

10

11 *Corresponding to: Zhouqing Xie (zqxie@ustc.edu.cn)

12

13 **Abstract.** The rapid mass increase of atmospheric nitrate is a critical driving force for the occurrence of fine-particle
14 pollution (referred to as haze hereafter) in Beijing. However, the exact mechanisms for this rapid increase of nitrate mass has
15 been not well constrained from field observations. Here we present the first observations of the oxygen-17 excess of
16 atmospheric nitrate ($\Delta^{17}\text{O}(\text{NO}_3^-)$) collected in Beijing haze to reveal the relative importance of different nitrate formation
17 pathways, and we also present the simultaneously observed $\delta^{15}\text{N}(\text{NO}_3^-)$. During our sampling period, 12h-averaged mass
18 concentrations of $\text{PM}_{2.5}$ varied from 16 to 323 $\mu\text{g m}^{-3}$ with a mean of $(141 \pm 88 \text{ (1SD)}) \mu\text{g m}^{-3}$, with nitrate ranging from 0.3
19 to 106.7 $\mu\text{g m}^{-3}$. The observed $\Delta^{17}\text{O}(\text{NO}_3^-)$ ranged from 27.5 ‰ to 33.9 ‰ with a mean of $(30.6 \pm 1.8) \text{‰}$ while $\delta^{15}\text{N}(\text{NO}_3^-)$
20 ranged from -2.5‰ to 19.2 ‰ with a mean of $(7.4 \pm 6.8) \text{‰}$. $\Delta^{17}\text{O}(\text{NO}_3^-)$ -constrained calculations suggest nocturnal
21 pathways ($\text{N}_2\text{O}_5 + \text{H}_2\text{O}/\text{Cl}^-$ and $\text{NO}_3 + \text{HC}$) dominated nitrate production during polluted days ($\text{PM}_{2.5} \geq 75 \mu\text{g m}^{-3}$) with the
22 mean possible fraction of 56 – 97 %. Our results illustrate the potentiality of $\Delta^{17}\text{O}$ in tracing nitrate formation pathways,
23 future modelling work with the constraint of isotope data reported here may further improve our understanding of nitrogen
24 cycle during haze.

25 1 Introduction

26 Severe and frequent haze pollution has become a crucial threat for the air quality in megacity Beijing and the North
27 China Plain in recent years. The high concentrations of $\text{PM}_{2.5}$ (particulate matter with an aerodynamic diameter equal or
28 less than 2.5 μm) during severe haze, of which the hourly average can reach 1000 $\mu\text{g m}^{-3}$ (Zheng et al., 2015a), is harmful

29 to the public health by contributing to cardiovascular morbidity and mortality (Cheng et al., 2013; Brook et al., 2010).
30 Nitrate is an important component of PM_{2.5}, accounting for 1–45 % of PM_{2.5} mass in Beijing and North China Plain (Wen et
31 al., 2015; Zheng et al., 2015a; Zheng et al., 2015b). The main formation pathways of atmospheric nitrate in urban area are
32 summarized in Fig. 1, which includes: (i) NO₂ oxidation by OH radical in the gas-phase, (ii) heterogeneous uptake of NO₂ on
33 wet aerosols, (iii) NO₃ radical reacting with hydrocarbon (HC), and (iv) heterogeneous uptake of N₂O₅ on wet aerosols and
34 chlorine-containing aerosols. Since OH radical is mainly present in the daytime while NO₃ radical and N₂O₅ are mainly
35 present in the nocturnal atmosphere (Brown and Stutz, 2012), NO₂ + OH is usually referred as the daytime nitrate formation
36 pathway while N₂O₅ + H₂O/Cl⁻ and NO₃ + HC are referred as nocturnal formation pathways (Vicars et al., 2013; Sofen et al.,
37 2014). During haze in Beijing, the mixing ratio of daytime OH is modelled to be low (Zheng et al., 2015b; Rao et al., 2016)
38 while relatively high mixing ratio of nocturnal N₂O₅ is observed in several studies (Wang et al., 2017a; Li et al., 2018; Wang
39 et al., 2017b), therefore, nocturnal pathways are suggested to be most responsible for the high concentrations of atmospheric
40 nitrate during haze (Su et al., 2017; Pathak et al., 2009; Pathak et al., 2011). In addition, the high PM_{2.5} concentration and
41 relative humidity during haze in Beijing favors heterogeneous reactions, which renders NO₂ + H₂O being a potentially
42 significant pathway for nitrate production (Wang et al., 2017d; Tong et al., 2015; Zheng et al., 2015a).

43 Nitrogen isotopic composition of nitrate ($\delta^{15}\text{N}(\text{NO}_3^-)$, wherein $\delta^{15}\text{N} = (R_{\text{sample}}/R_{\text{reference}} - 1)$ with R representing isotope
44 ratios of $^{15}\text{N}/^{14}\text{N}$ in the sample and the reference atmospheric N₂) is useful in tracing source of its precursor NO_x (Xiao et al.,
45 2015; Beyn et al., 2014; Fang et al., 2011; Hastings et al., 2013). Anthropogenic sources of NO_x such as coal combustion are
46 generally enriched in $\delta^{15}\text{N}$ while natural NO_x sources such as soil emissions or lightning typically have negative or zero $\delta^{15}\text{N}$
47 signature (Hoering, 1957; Yu and Elliott, 2017; Felix et al., 2012). Therefore highly positive values of observed $\delta^{15}\text{N}(\text{NO}_3^-)$
48 can be considered as an indicator of anthropogenic combustion (Elliott et al., 2009; Fang et al., 2011), although this
49 judgment may be influenced by isotopic exchange between NO and NO₂ (Freyer et al., 1993; Walters et al., 2016), **isotopic**
50 **fractionations associated with nitrate formation pathways and isotopic effects occurring during transport, such as deposition**
51 **of NO₃⁻ and HNO₃ partitioning between gas and particle phase (Freyer, 1991; Geng et al., 2014).** The oxygen-17 excess
52 ($\Delta^{17}\text{O}$) of nitrate, defined as $\Delta^{17}\text{O} = \delta^{17}\text{O} - 0.52\delta^{18}\text{O}$, wherein $\delta^{\text{X}}\text{O} = (R_{\text{sample}}/R_{\text{reference}} - 1)$ with R representing isotope ratios
53 of $^{\text{X}}\text{O}/^{16}\text{O}$ in the sample and the reference Vienna Standard Mean Ocean Water and X = 17 or 18, is particularly useful in
54 reflecting nitrate formation pathways (Michalski et al., 2003). Atmospheric nitrate from nocturnal reaction pathways has
55 higher $\Delta^{17}\text{O}$ than that from daytime OH oxidation at given $\Delta^{17}\text{O}(\text{NO}_2)$ (Table 1). **And once formed**, atmospheric $\Delta^{17}\text{O}(\text{NO}_3^-)$
56 cannot be altered by mass-dependent processes such as deposition during transport (Brenninkmeijer et al., 2003). Previous
57 studies have shown the utility of atmospheric $\Delta^{17}\text{O}(\text{NO}_3^-)$ in quantifying the relative importance of various nitrate formation
58 pathways (Alexander et al., 2009; Michalski et al., 2003; Patris et al., 2007; Savarino et al., 2013; Vicars et al., 2013). For
59 example, $\Delta^{17}\text{O}(\text{NO}_3^-)$ -constrained box modeling work of Michalski et al. (2003) suggests that more than 90 % of

60 atmospheric nitrate is from nocturnal $\text{N}_2\text{O}_5 + \text{H}_2\text{O}$ pathway in winter La Jolla, California, which is reflected by the highest
61 $\Delta^{17}\text{O}(\text{NO}_3^-)$ values being observed in winter. In another study, Alexander et al. (2009) use observed $\Delta^{17}\text{O}(\text{NO}_3^-)$ to constrain
62 3D model and found that daytime $\text{NO}_2 + \text{OH}$ pathway dominates global tropospheric nitrate production with an annual mean
63 contribution of 76 %.

64 Until now, however, field observations of atmospheric $\Delta^{17}\text{O}(\text{NO}_3^-)$ have not been conducted in north China to constrain
65 the relative importance of different nitrate formation pathways during haze. In this work, we present the first observations of
66 atmospheric $\Delta^{17}\text{O}(\text{NO}_3^-)$ during Beijing haze from October 2014 to January 2015, and use this observation to examine the
67 importance of nocturnal formation pathways. We also present the signature of simultaneously observed $\delta^{15}\text{N}(\text{NO}_3^-)$.

68 **2 Materials and Methods**

69 **2.1 Sampling and atmospheric observations**

70 $\text{PM}_{2.5}$ filter samples were collected at a flow rate of $1.05 \text{ m}^3 \text{ min}^{-1}$ by a high volume air sampler (model TH-1000C II,
71 Tianhong Instruments Co., Ltd, China). The filter is quartz microfiber filter (Whatman Inc., UK), pre-combusted at 450°C
72 for 4 h before sampling. Our sampling period lasted from October 2014 to January 2015 with the collection interval being 12
73 h (08:00 – 20:00 LT or 20:00 – 08:00 LT) for each sample. Blank control samples were also collected. The blank was
74 sampled identically to the real sample except that the collection interval is 1 min. Due to that gaseous HNO_3 is likely to
75 adsorb onto particulate matter already trapped by the filter material (Vicars et al., 2013), the nitrate species collected is likely
76 to include both particulate nitrate and gaseous HNO_3 , which is referred to as atmospheric nitrate in previous studies (Vicars
77 et al., 2013; Morin et al., 2009; Michalski et al., 2003) and in this study. The **sampling site** is at the campus of University of
78 the Chinese Academy of Sciences (40.41°N , 116.68°E , ~ 20 m high) in suburban Beijing, about 60 km northeast of
79 downtown (Fig. 2), which is **a super site set by HOPE-J³A** (Haze Observation Project Especially for Jing-Jin-Ji Area) with
80 various observations being reported (Zhang et al., 2017; Xu et al., 2016; Chen et al., 2015; Tong et al., 2015; He et al., 2018).
81 Hourly concentrations of surface $\text{PM}_{2.5}$, CO , SO_2 , NO_2 and O_3 were observed at Huairou station (40.33°N , 116.63°E) by
82 Beijing Municipal Environmental Monitoring Center, **about 10 km to our sampling site**. Meteorological data including
83 relative humidity (RH) and air temperature (T) were measured by an automatic weather station (model MetPak, Gill
84 Instruments Limited, UK). Time used in the present study is local time (LT = UTC + 8).

85 **2.2 Measurements of ions and isotopic ratios**

86 Ion concentrations of NO_3^- and Cl^- were measured in Anhui Province Key Laboratory of Polar Environment and Global

87 Change in the University of Science and Technology of China. A detailed description of this method can be found in the
 88 literature (Ye et al., 2015). Briefly, ions in the PM_{2.5} filter sample were extracted with Millipore water ($\geq 18 \text{ M}\Omega$) and
 89 insoluble substances in the extract were filtered. Then the ion concentrations were analyzed by an ion chromatograph system
 90 (model Dionex ICS-2100, Thermo Fisher Scientific Inc., USA). The measured ion concentrations of blank samples were
 91 subtracted when determining the ion concentrations of real samples. Typical analytical precision by our method is better than
 92 10 % relative standard deviation (RSD) (Chen et al., 2016).

93 $\delta^{15}\text{N}(\text{NO}_3^-)$ and $\Delta^{17}\text{O}(\text{NO}_3^-)$ were measured with a bacterial denitrifier method (Kaiser et al., 2007) in IsoLab at the
 94 University of Washington, USA. Briefly, ions in the filter sample were extracted with Millipore water ($\geq 18 \text{ M}\Omega$) and the
 95 insoluble substances were filtered. NO_3^- in each sample was converted to N_2O by the denitrifying bacteria, *Pseudomonas*
 96 *aureofaciens*. Then N_2 and O_2 , which were decomposed from N_2O in a gold tube at 800°C , were separated by a gas
 97 chromatograph. The isotopic ratios of each gas were then measured by a Finnigan Delta-Plus Advantage isotope ratio mass
 98 spectrometer. Masses of 28 and 29 from N_2 were measured to determine $\delta^{15}\text{N}$. Masses of 32, 33 and 34 from O_2 were
 99 measured to determine $\delta^{17}\text{O}$ and $\delta^{18}\text{O}$ and $\Delta^{17}\text{O}$ was then calculated. We use international nitrate reference materials,
 100 USGS34, USGS35 and IAEANO₃, for data calibration. The uncertainty (1σ) of $\delta^{15}\text{N}$ and $\Delta^{17}\text{O}$ measurements in our method
 101 is 0.4 ‰ and 0.2 ‰, respectively, based on replicate analysis of the international reference materials. All the samples
 102 including blank samples were measured in triplicate to quantify the uncertainty in each sample. The blank was subtracted for
 103 each sample by using an isotopic mass balance on the basis of isotopic ratios and concentrations of the blank. To minimize
 104 the blank effect, samples with blank concentrations being $> 10\%$ of their concentrations were not analyzed for isotopic
 105 ratios. This ruled out 3 of the total 34 samples, all of which are in non-polluted days (NPD, $\text{PM}_{2.5} < 75 \mu\text{g m}^{-3}$). Totally,
 106 isotopic compositions of 7 samples in NPD and 24 samples in polluted days (PD, $\text{PM}_{2.5} \geq 75 \mu\text{g m}^{-3}$) are reported here.

107 2.3 Estimate of different nitrate formation pathways based on $\Delta^{17}\text{O}(\text{NO}_3^-)$

108 The observed $\Delta^{17}\text{O}(\text{NO}_3^-)$ is determined by the relative importance of different nitrate formation pathways and the
 109 relative importance of O_3 oxidation in NO_x cycling as shown in Eq. (1):

$$110 \Delta^{17}\text{O}(\text{NO}_3^-) = \Delta^{17}\text{O}_{\text{R6}} \times f_{\text{R6}} + \Delta^{17}\text{O}_{\text{R7}} \times f_{\text{R7}} + \Delta^{17}\text{O}_{\text{R8}} \times f_{\text{R8}} + \Delta^{17}\text{O}_{\text{R9}} \times f_{\text{R9}} + \Delta^{17}\text{O}_{\text{R10}} \times f_{\text{R10}} \quad (1)$$

111 Where $\Delta^{17}\text{O}_{\text{R6}}$, $\Delta^{17}\text{O}_{\text{R7}}$, $\Delta^{17}\text{O}_{\text{R8}}$, $\Delta^{17}\text{O}_{\text{R9}}$ and $\Delta^{17}\text{O}_{\text{R10}}$ is respectively $\Delta^{17}\text{O}(\text{NO}_3^-)$ resulting from $\text{NO}_2 + \text{OH}$, $\text{NO}_2 + \text{H}_2\text{O}$, $\text{NO}_3 +$
 112 HC , $\text{N}_2\text{O}_5 + \text{H}_2\text{O}$ and $\text{N}_2\text{O}_5 + \text{Cl}^-$ pathway (Table 1). f_{R6} , f_{R7} , f_{R8} , f_{R9} and f_{R10} is respectively corresponding fractional
 113 contribution of above pathways to nitrate production. By using the $\Delta^{17}\text{O}$ assumptions for different pathways in Table 1 and
 114 the definition $f_{\text{R6}} + f_{\text{R7}} + f_{\text{R8}} + f_{\text{R9}} + f_{\text{R10}} = 1$, Eq. (1) is further expressed as:

$$115 \Delta^{17}\text{O}(\text{NO}_3^-)/\text{‰} = 25\alpha f_{\text{R6}} + 25\alpha f_{\text{R7}} + (25\alpha + 14) \times f_{\text{R8}} + (25\alpha + 7) \times f_{\text{R9}} + (25\alpha + 14) \times f_{\text{R10}} = 25\alpha + 14 \times$$

$$116 (f_{\text{R8}} + f_{\text{R10}}) + 7f_{\text{R9}} \quad (2)$$

117 Where α is the proportion of O_3 oxidation in NO_2 production rate, calculated by Eq. (3):

$$118 \alpha = \frac{k_{R1}[NO][O_3]}{k_{R1}[NO][O_3] + k_{R2a}[NO][HO_2] + k_{R2b}[NO][RO_2]} \quad (3)$$

119 In Eq. (3), k_{R1} , k_{R2a} and k_{R2b} is respectively the reaction rate constant listed in Table 2. To evaluate α , we estimated HO_2
120 mixing ratios on the basis of empirical formulas between HO_2 and O_3 mixing ratios derived from observations in winter
121 (Kanaya et al., 2007), that's: $[HO_2]/(pmol\ mol^{-1}) = \exp(5.7747 \times 10^{-2} \times [O_3]/(nmol\ mol^{-1}) - 1.7227)$ during the day time and
122 $[HO_2]/(pmol\ mol^{-1}) = \exp(7.7234 \times 10^{-2} \times [O_3]/(nmol\ mol^{-1}) - 1.6363)$ at night. Then RO_2 mixing ratio was calculated as 70 %
123 of HO_2 mixing ratios based on previous studies (Liu et al., 2012; Elshorbany et al., 2012; Mihelcic et al., 2003). As NO
124 mixing ratio was not observed in our study, we estimated NO mixing ratios following the empirical formulas between NO_x
125 and CO mixing ratios derived from observations in winter Beijing (Lin et al., 2011), that's: $[NO]/(nmol\ mol^{-1}) =$
126 $([CO]/(nmol\ mol^{-1}) - 196)/27.3 - [NO_2]/(nmol\ mol^{-1})$ during daytime and $[NO]/(nmol\ mol^{-1}) = ([CO]/(nmol\ mol^{-1}) -$
127 $105)/30.9 - [NO_2]/(nmol\ mol^{-1})$ at night.

128 By using Eq. (2), the relative importance of nocturnal formation pathways ($f_{R8} + f_{R9} + f_{R10}$) can be written as Eq. (4):

$$129 f_{R8} + f_{R9} + f_{R10} = \frac{f_{R9}}{2} + \frac{\Delta^{17}O(NO_3^-)}{14\text{‰}} - 1.8\alpha \quad (4)$$

130 Eq. (4) suggests that the relative importance of nocturnal pathways is solely a function of the assumption of f_{R9} at given
131 $\Delta^{17}O(NO_3^-)$ and α . Since f_{R9} , $f_{R8} + f_{R10}$ and $f_{R8} + f_{R9} + f_{R10}$ should be in the range of 0 – 1 **all the time**, f_{R9} is further limited to
132 meet Eq. (5):

$$133 f_{R9} \begin{cases} > 0 \\ < \min(1, \frac{\Delta^{17}O(NO_3^-)}{7\text{‰}} - 3.6\alpha, 2 + 3.6\alpha - \frac{\Delta^{17}O(NO_3^-)}{7\text{‰}}) \end{cases} \quad (5)$$

134 We estimated the relative importance of nocturnal pathways ($f_{R8} + f_{R9} + f_{R10}$) by using concentration-weighted
135 $\Delta^{17}O(NO_3^-)$ observations and production rate weighted α in PD of each haze event rather than each sample due to the
136 lifetime of atmospheric nitrate is typically on the order of day (Liang et al., 1998), larger than our sampling collection
137 interval.

138 2.4 Simulation of surface N_2O_5 and NO_3 radical

139 **To see whether the relative importance of nocturnal pathways constrained by $\Delta^{17}O(NO_3^-)$ can be reproduced by models,**
140 we use the standard Master Chemical Mechanism (MCM, version 3.3, <http://mcm.leeds.ac.uk/>) to simulate the mixing
141 ratios of surface N_2O_5 and NO_3 radical during our sampling period. The input for this modeling work includes: (i) 1
142 h-averaged mixing ratios of observed surface CO , NO_2 , SO_2 and O_3 and estimated NO (see Sect. 2.3), (ii) observed RH and
143 T , and (iii) the mixing ratios of organic compounds from the literatures (Table S1) (Wang et al., 2001; Wu et al., 2016; Rao et
144 al., 2016).

146 3.1 Overview of observations in Beijing haze

147 Figure 3 describes general characteristics of haze events during our observations. The 12h-averaged $PM_{2.5}$
 148 concentrations, corresponding with filter samples, varied from 16 to 323 $\mu\text{g m}^{-3}$ with a mean of $(141 \pm 88 \text{ (1SD)}) \mu\text{g m}^{-3}$. In
 149 comparison, the Grade II of NAAQS (National Ambient Air Quality Standard) in China is 75 $\mu\text{g m}^{-3}$ for daily $PM_{2.5}$. The
 150 NO_3^- concentrations present similar trends with $PM_{2.5}$ levels (Fig. 3a), ranged from 0.3 to 106.7 $\mu\text{g m}^{-3}$ with a mean of
 151 $(6.1 \pm 5.3) \mu\text{g m}^{-3}$ in non-polluted days (NPD, $PM_{2.5} < 75 \mu\text{g m}^{-3}$) and $(48.4 \pm 24.7) \mu\text{g m}^{-3}$ in polluted days (PD, $PM_{2.5} \geq 75 \mu\text{g}$
 152 m^{-3}). Correspondingly, the nitrogen oxidation ratio (NOR, which equals to NO_3^- molar concentration divided by the sum of
 153 NO_3^- and NO_2 molar concentration), a proxy for secondary transformation of nitrate (Sun et al., 2006), increased from a
 154 mean of 0.09 ± 0.05 in NPD to 0.31 ± 0.10 in PD (Fig. 3b). In residential heating season (Case III – V in November 2014 –
 155 January 2015, Fig. 3b), Cl^- concentrations present similar trends with NO_3^- levels, increased from $(0.6 \pm 1.0) \mu\text{g m}^{-3}$ in NPD
 156 to $(7.9 \pm 4.8) \mu\text{g m}^{-3}$ in PD. However, during Case I – II in October 2014, Cl^- concentrations were $(3.5 \pm 1.6) \mu\text{g m}^{-3}$ in NPD
 157 and $(3.5 \pm 1.9) \mu\text{g m}^{-3}$ in PD, showing no significant difference at 0.01 level (t-test). Throughout our observational period, the
 158 visibility decreased from $(11.4 \pm 6.7) \text{ km}$ in NPD to $(3.1 \pm 1.8) \text{ km}$ in PD (Fig. 3c) while relative humidity (RH) increased from
 159 $(37 \pm 12) \%$ in NPD to $(62 \pm 12) \%$ in PD (Fig. 3d).

160 $\Delta^{17}O(NO_3^-)$ ranged from 27.5 ‰ to 33.9 ‰ with the mean of $(29.1 \pm 1.3) \%$ in NPD and $(31.0 \pm 1.7) \%$ in PD (Fig. 3c).
 161 Our observed $\Delta^{17}O(NO_3^-)$ is in the range of $\Delta^{17}O(NO_3^-)$ reported in literatures (Table 3) but at the high end of values from
 162 other non-polar regions (Table 3). All our observed $\Delta^{17}O(NO_3^-)$ values, no matter daytime sample (08:00 – 20:00) or
 163 nighttime sample (20:00 – 08:00), are larger than 25 ‰, the maximum of $\Delta^{17}O(NO_3^-)$ that can be produced via $NO_2 + OH$
 164 and $NO_2 + H_2O$ (Table 1) at the assumption of bulk $\Delta^{17}O(O_3) = 26 \%$ (Ishino et al., 2017; Vicars and Savarino, 2014). This
 165 directly suggests nocturnal formation pathways ($N_2O_5 + H_2O/Cl^-$ and $NO_3 + HC$) must contribute to all the sampled nitrate.
 166 Given the lifetime of atmospheric nitrate is typically larger than our sampling collection interval (Vicars et al., 2013), **each of**
 167 **our samples** is expected to reflect both daytime and nocturnal nitrate production. Not surprisingly, $\Delta^{17}O(NO_3^-)$ mean of
 168 daytime and nighttime samples is $(30.3 \pm 1.5) \%$ and $(30.9 \pm 2.1) \%$, respectively, showing no significant difference at 0.01
 169 level (t-test).

170 $\delta^{15}N(NO_3^-)$ in our observation varied from -2.5% to 19.2 ‰ with a mean of $(7.4 \pm 6.8) \%$, which is in the range of
 171 $\delta^{15}N(NO_3^-)$ observed from rainwater in Beijing, China (Zhang et al., 2008) and similar to $\delta^{15}N(NO_3^-)$ values observed from
 172 aerosols in Germany (Freyer, 1991). Figure 3d shows that $\delta^{15}N(NO_3^-)$ varies largely in October 2014. The mean $\delta^{15}N(NO_3^-)$
 173 varied from $(0.4 \pm 1.5) \%$ in 08:00 Oct. 18 – 08:00 Oct. 21 to $(10.7 \pm 1.4) \%$ in 08:00 Oct. 21 – 08:00 Oct. 23 and then

174 decreased to (-0.9 ± 2.1) ‰ in 08:00 Oct. 23 – 08:00 Oct. 26, which corresponds to $PM_{2.5}$ concentrations being 155 ± 63 ,
175 57 ± 19 and (188 ± 51) $\mu\text{g m}^{-3}$ respectively. However, during residential heating season, relatively high $\delta^{15}\text{N}(\text{NO}_3^-)$ ($7.6 -$
176 19.2 ‰) were always observed both in NPD and PD. This may be related to the high NO_x emission from coal combustion in
177 north China (Wang et al., 2012; Lin, 2012; Zhang et al., 2007).

178 3.2 Relationships between $\Delta^{17}\text{O}(\text{NO}_3^-)$ and other data

179 Figure 4 presents the relationships between $\Delta^{17}\text{O}(\text{NO}_3^-)$ and NO_3^- concentrations, $PM_{2.5}$ concentrations, NOR, visibility,
180 RH and $\delta^{15}\text{N}(\text{NO}_3^-)$. $\Delta^{17}\text{O}(\text{NO}_3^-)$ shows a positive correlation with NO_3^- concentrations when $\text{NO}_3^- < 50$ $\mu\text{g m}^{-3}$ ($r = 0.81$, p
181 < 0.01). Similarly, $\Delta^{17}\text{O}(\text{NO}_3^-)$ shows a positive correlation with $PM_{2.5}$ concentration in Fig. 4b and NOR in Fig. 4c when
182 $\text{NO}_3^- < 50$ $\mu\text{g m}^{-3}$ ($r = 0.71$ and $r = 0.80$, $p < 0.01$, respectively). Figure 4d shows that $\Delta^{17}\text{O}(\text{NO}_3^-)$ is negative correlated with
183 visibility in general ($r = -0.66$, $p < 0.01$). The significant decrease of visibility will largely reduce surface radiation and
184 thereby OH mixing ratios (Zheng et al., 2015b), which is unfavorable for nitrate production via $\text{NO}_2 + \text{OH}$ pathway. Since
185 $\text{NO}_2 + \text{OH}$ pathway produces low $\Delta^{17}\text{O}(\text{NO}_3^-)$ (Table 1), the decreased importance of $\text{NO}_2 + \text{OH}$ pathway will conversely
186 increase $\Delta^{17}\text{O}(\text{NO}_3^-)$. While the raise of RH accompanying the large increase of $PM_{2.5}$ favors nitrate production via
187 heterogeneous uptake of gases, e.g., N_2O_5 (Zheng et al., 2015b; Zheng et al., 2015a) and heterogeneous uptake of N_2O_5
188 produces relative high $\Delta^{17}\text{O}(\text{NO}_3^-)$ (Table 1), the enhanced heterogeneous uptake of N_2O_5 will increase $\Delta^{17}\text{O}(\text{NO}_3^-)$ too.
189 Therefore, the decrease of importance of $\text{NO}_2 + \text{OH}$ and the increase of importance of heterogeneous uptake of N_2O_5 should
190 be responsible for the positive correlation between $\Delta^{17}\text{O}(\text{NO}_3^-)$ and NO_3^- concentrations. In addition, for samples with $\text{NO}_3^- >$
191 50 $\mu\text{g m}^{-3}$, visibility was always low with narrow variations (2.3 ± 1.0 km) and RH was always high with narrow range
192 (67 ± 7 ‰), which may be responsible for the relatively high $\Delta^{17}\text{O}(\text{NO}_3^-)$ being observed (31.2 ± 1.7 ‰). Figure 4f shows that
193 $\Delta^{17}\text{O}(\text{NO}_3^-)$ is not correlated with $\delta^{15}\text{N}(\text{NO}_3^-)$.

194 3.3 Estimate of nocturnal formation pathways

195 Before estimating the relative importance of different nitrate formation pathways, we estimate the proportion of O_3
196 oxidation in NO_2 production rate, α . The possible α range can be calculated based on observed $\Delta^{17}\text{O}(\text{NO}_3^-)$. It can be
197 obtained from Table 1 that 25α ‰ $< \Delta^{17}\text{O}(\text{NO}_3^-) < (25\alpha + 14)$ ‰, so the lower limit of possible α is $(\Delta^{17}\text{O}(\text{NO}_3^-) -$
198 14 ‰)/ 25 ‰. And since $\Delta^{17}\text{O}(\text{NO}_3^-) \geq 27.5$ ‰ in our observation, the higher limit of α is always 1 for all the samples. Figure
199 5 presents the possible range of calculated α based on $\Delta^{17}\text{O}(\text{NO}_3^-)$. The calculated lower limit of α ranged from 0.56 to 0.81
200 with a mean of 0.68 ± 0.07 , which directly suggests that O_3 oxidation played a dominated role in NO_x cycling during Beijing
201 haze. To estimate the specific α value, chemical kinetics in Table 2 and Eq. (3) were used. Specific α is estimated to range
202 from 0.86 to 0.97 with a mean of (0.94 ± 0.03) , which is in the possible range of α value calculated directly based on

203 $\Delta^{17}\text{O}(\text{NO}_3^-)$ (Fig. 5) and close to the range of 0.85 – 1 determined in other mid-latitude areas (Michalski et al., 2003; Patris et
204 al., 2007).

205 Figure 6a shows the estimated relative importance of nocturnal formation pathways ($\text{N}_2\text{O}_5 + \text{H}_2\text{O}/\text{Cl}^-$ and $\text{NO}_3 + \text{HC}$)
206 during PD of each case on the basis of observed $\Delta^{17}\text{O}(\text{NO}_3^-)$. Possible fractional contribution of nocturnal formation
207 pathways ranges from 49 – 97 %, 58 – 100 %, 60 – 100 %, 45 – 90 % and 70 – 100 % in PD of Case I to V, respectively,
208 with a mean of 56 – 97 %. This directly implies that nocturnal chemistry dominates atmospheric nitrate production in Beijing
209 haze. This finding is consistent with the suggested importance of heterogeneous uptake of N_2O_5 during Beijing haze by
210 previous studies (Su et al., 2017; Wang et al., 2017b). The other pathways ($\text{NO}_2 + \text{OH}$ and $\text{NO}_2 + \text{H}_2\text{O}$) account for the
211 remaining fraction with a mean possible range of 3 – 44 %. Since $\text{NO}_2 + \text{OH}$ and $\text{NO}_2 + \text{H}_2\text{O}$ produces the same $\Delta^{17}\text{O}(\text{NO}_3^-)$
212 signature in our assumptions (Table 1), we cannot distinguish their fractional contribution barely from the observed
213 $\Delta^{17}\text{O}(\text{NO}_3^-)$ in the present study. However, the overall positive correlation between $\Delta^{17}\text{O}(\text{NO}_3^-)$ and RH ($r = 0.55$, $p < 0.01$,
214 Fig. 4e) suggests heterogeneous uptake of NO_2 should be less important than heterogeneous uptake of N_2O_5 , otherwise, a
215 negative relationship between $\Delta^{17}\text{O}(\text{NO}_3^-)$ and RH is expected. Our calculations also suggest that the sum of possible
216 fractional contribution of $\text{N}_2\text{O}_5 + \text{Cl}^-$ and $\text{NO}_3 + \text{HC}$ is in the range of 0 – 49 %, 17 – 58 %, 20 – 60 %, 0 – 45 % and 41 – 70 %
217 in PD of Case I to V, respectively, with a mean of 16 – 56 % (Table 4), which emphasizes that $\text{N}_2\text{O}_5 + \text{Cl}^-$ and $\text{NO}_3 + \text{HC}$
218 played a non-ignorable role in nitrate production during Beijing haze. Due to that $\text{N}_2\text{O}_5 + \text{Cl}^-$ and $\text{NO}_3 + \text{HC}$ produce the
219 same $\Delta^{17}\text{O}(\text{NO}_3^-)$ in our assumptions (Table 1), we cannot distinguish their fractional contribution barely from the observed
220 $\Delta^{17}\text{O}(\text{NO}_3^-)$ in this study, either. However, $\text{NO}_3 + \text{HC}$ should be minor for nitrate production. For example, 3D modelling
221 work of Alexander et al. (2009) suggests $\text{NO}_3 + \text{HC}$ pathway only accounts for 4 % of global tropospheric nitrate production
222 annually on average, and Michalski et al. (2003) found that $\text{NO}_3 + \text{HC}$ pathway contributes 1 – 10 % to nitrate production on
223 the basis of an annual observation at La Jolla, California, with low values in winter. Therefore, in addition to $\text{NO}_3 + \text{HC}$,
224 $\text{N}_2\text{O}_5 + \text{Cl}^-$ is likely to also contribute to nitrate production during haze in Beijing. Supportively, the concentrations of Cl^- is
225 as high as $(5.5 \pm 4.1) \mu\text{g m}^{-3}$ during PD of all the cases in our observation and the mixing ratios of ClNO_2 , an indicator of
226 $\text{N}_2\text{O}_5 + \text{Cl}^-$ pathway, reached up to $2.9 \text{ nmol mol}^{-1}$ during a summer observation in suburban Beijing (Wang et al., 2018b)
227 and reached up to $5.0 \text{ nmol mol}^{-1}$ in a modelling work in summer rural Beijing (Wang et al., 2017c).

228 Figure 6b presents the simulated mixing ratios of surface N_2O_5 and NO_3 radical during our observational period by
229 using the box model MCM. The 12h averaged mixing ratios of simulated N_2O_5 ranged from 3 to $649 \text{ pmol mol}^{-1}$ while
230 simulated NO_3 radical ranged from 0 to 27 pmol mol^{-1} . In comparison, previous observations in Beijing suggest 5s averaged
231 N_2O_5 can be as high as $1.3 \text{ nmol mol}^{-1}$ and 30 min averaged NO_3 radical can be as high as 38 pmol mol^{-1} with large
232 day-to-day variability (Wang et al., 2017b; Wang et al., 2015). During Case I and II in October, simulated N_2O_5 and NO_3
233 radical present similar trends with the observed NO_3^- and remain relatively high during PD ($346 \pm 128 \text{ pmol mol}^{-1}$ and 9 ± 7

234 pmol mol⁻¹, respectively, Fig. 6b), which supports the dominant role of nocturnal formation pathways suggested by
235 $\Delta^{17}\text{O}(\text{NO}_3^-)$. However, during Case III – V in residential heating season, the simulated surface mixing ratios of N₂O₅ and
236 NO₃ radical remain relatively low during PD (63±80 pmol mol⁻¹ and < 1 pmol mol⁻¹, respectively, Fig. 6b), which seems to
237 be inconsistent with $\Delta^{17}\text{O}(\text{NO}_3^-)$ observations. We note that a recent study suggests that heterogeneous uptake of N₂O₅ is
238 negligible at surface but larger at higher altitudes (e.g., > 150 m) during winter haze in Beijing (Wang et al., 2018a). So
239 during PD of Case III – V in our observational period, large nitrate production via heterogeneous uptake of N₂O₅ may occur
240 aloft rather than at surface, which leads to the dominant role of nocturnal formation pathways as suggested by $\Delta^{17}\text{O}(\text{NO}_3^-)$.

241 4 Conclusions

242 We report the first observation of isotopic composition ($\Delta^{17}\text{O}$ and $\delta^{15}\text{N}$) of atmospheric nitrate in Beijing haze. The
243 observed $\Delta^{17}\text{O}(\text{NO}_3^-)$ ranged from 27.5 ‰ to 33.9 ‰ with a mean of (30.6±1.8) ‰. $\delta^{15}\text{N}(\text{NO}_3^-)$ ranged largely from -2.5 ‰
244 to 19.2 ‰ with a mean of (7.4±6.8) ‰. When NO₃⁻ is < 50 μg m⁻³, a positive correlation was observed between $\Delta^{17}\text{O}(\text{NO}_3^-)$
245 and NO₃⁻ concentration (r = 0.81, p < 0.01). This is likely to result from the variation of relative importance of different
246 nitrate formation pathway. **Calculations with the constraint of $\Delta^{17}\text{O}(\text{NO}_3^-)$ suggest that nocturnal pathways (N₂O₅ + H₂O/Cl⁻
247 and NO₃ + HC) dominated nitrate production during polluted days (PM_{2.5} ≥ 75 μg m⁻³), with the mean possible contribution
248 of 56 – 97 %. $\Delta^{17}\text{O}(\text{NO}_3^-)$ also indicates that O₃ dominated NO oxidation during Beijing haze.**

249 Supplementary Materials

250 **Figure S1.** The diurnal differences of observed NO₂, CO and O₃ and calculated NO, HO₂ and RO₂ during our sampling
251 periods.

252 **Table S1.** The input of organic compounds for MCM model (nmol mol⁻¹).

253 Data availability

254 All data needed to draw the conclusions are present in the main text and/or the Supplementary Materials. For additional
255 data, please contact the corresponding author (zqxie@ustc.edu.cn).

256 **Author contributions**

257 Z.Q.X. conceived this study. P.Z.H. conducted isotope measurements. P.Z.H., X.Y.C, S.D.F, H.C.Z., H. K. performed
258 the field experiments and ion measurements. P.Z.H., Z.Q.X., X.W.Y. interpreted the data. C.L. contributed to the field
259 observation support. P.Z.H. wrote the manuscript with Z.Q.X. inputs. All authors involved the discussion and revision.

260 **Competing interests**

261 The authors declare no competing interests.

262 **Acknowledgments**

263 This work was supported by the National Key Project of MOST (2016YFC0203302), NSFC (91544013), the Key
264 Project of CAS (KJZD-EW-TZ-G06-01) and the Atmospheric Pollution Control of the Prime Minister (DQGG0104). We
265 gratefully thank staffs of IsoLab at UW for their technical support, Becky Alexander and Lei Geng for helpful discussions.

266 **References**

- 267 Alexander, B., Hastings, M. G., Allman, D. J., Dachs, J., Thornton, J. A., and Kunasek, S. A.: Quantifying atmospheric
268 nitrate formation pathways based on a global model of the oxygen isotopic composition ($\Delta^{17}\text{O}$) of atmospheric nitrate,
269 *Atmos. Chem. Phys.*, 9, 5043-5056, 2009.
- 270 Berhanu, T. A., Savarino, J., Bhattacharya, S. K., and Vicars, W. C.: ^{17}O excess transfer during the $\text{NO}_2 + \text{O}_3 \rightarrow \text{NO}_3 + \text{O}_2$
271 reaction, *J. Chem. Phys.*, 136, 044311, 2012.
- 272 Bertram, T. H., and Thornton, J. A.: Toward a general parameterization of N_2O_5 reactivity on aqueous particles: the
273 competing effects of particle liquid water, nitrate and chloride, *Atmos. Chem. Phys.*, 9, 8351-8363, 2009.
- 274 Beyn, F., Matthias, V., and Dänke, K.: Changes in atmospheric nitrate deposition in Germany—An isotopic perspective,
275 *Environ. Pollut.*, 194, 1-10, 2014.
- 276 Brenninkmeijer, C. A., Janssen, C., Kaiser, J., Röckmann, T., Rhee, T. S., and Assonov, S. S.: Isotope effects in the chemistry
277 of atmospheric trace compounds, *Chem. Rev.*, 103, 5125-5162, 2003.
- 278 Brook, R. D., Rajagopalan, S., Pope, C. A., Brook, J. R., Bhatnagar, A., Diez-Roux, A. V., Holguin, F., Hong, Y., Luepker, R.
279 V., and Mittleman, M. A.: Particulate matter air pollution and cardiovascular disease an update to the scientific

280 statement from the American Heart Association, *Circulation*, 121, 2331-2378, 2010.

281 Brown, S. S., and Stutz, J.: Nighttime radical observations and chemistry, *Chem. Soc. Rev.*, 41, 6405-6447, 2012.

282 Burkholder, J. B., Sander, S. P., Abbatt, J. P. D., Barker, J. R., Huie, R. E., Kolb, C. E., Kurylo, M. J., Orkin, V. L., Wilmouth,
283 D. M., and Wine, P. H.: *Chemical Kinetics and Photochemical Data for Use in Atmospheric Studies: Evaluation*
284 *Number 18*, Pasadena, CA: Jet Propulsion Laboratory, National Aeronautics and Space Administration, 2015.

285 Chen, Q., Geng, L., Schmidt, J. A., Xie, Z., Kang, H., Dachs, J., Cole-Dai, J., Schauer, A. J., Camp, M. G., and Alexander, B.:
286 Isotopic constraints on the role of hypohalous acids in sulfate aerosol formation in the remote marine boundary layer,
287 *Atmos. Chem. Phys.*, 16, 11433-11450, 2016.

288 Chen, Z., Zhang, J., Zhang, T., Liu, W., and Liu, J.: Haze observations by simultaneous lidar and WPS in Beijing before and
289 during APEC, 2014, *Sci. China Chem.*, 58, 1385-1392, 2015.

290 Cheng, Z., Jiang, J., Fajardo, O., Wang, S., and Hao, J.: Characteristics and health impacts of particulate matter pollution in
291 China (2001–2011), *Atmos. Environ.*, 65, 186-194, 2013.

292 Cheung, J. L., Li, Y., Boniface, J., Shi, Q., Davidovits, P., Worsnop, D. R., Jayne, J. T., and Kolb, C. E.: Heterogeneous
293 interactions of NO₂ with aqueous surfaces, *J. Phys. Chem. A*, 104, 2655-2662, 2000.

294 Elliott, E. M., Kendall, C., Boyer, E. W., Burns, D. A., Lear, G. G., Golden, H. E., Harlin, K., Bytnerowicz, A., Butler, T. J.,
295 and Glatz, R.: Dual nitrate isotopes in dry deposition: Utility for partitioning NO_x source contributions to landscape
296 nitrogen deposition, *J. Geophys. Res. Biogeo.*, 114, 2009.

297 Elshorbany, Y. F., Kleffmann, J., Hofzumahaus, A., Kurtenbach, R., Wiesen, P., Brauers, T., Bohn, B., Dorn, H. P., Fuchs, H.,
298 and Holland, F.: HO_x budgets during HO_xComp: A case study of HO_x chemistry under NO_x - limited conditions, *J.*
299 *Geophys. Res.*, 117, 2012.

300 Fang, Y., Koba, K., Wang, X., Wen, D., Li, J., Takebayashi, Y., Liu, X., and Yoh, M.: Anthropogenic imprints on nitrogen and
301 oxygen isotopic composition of precipitation nitrate in a nitrogen-polluted city in southern China, *Atmos. Chem. Phys.*,
302 11, 1313-1325, 2011.

303 Felix, J. D., Elliott, E. M., and Shaw, S. L.: Nitrogen isotopic composition of coal-fired power plant NO_x: influence of
304 emission controls and implications for global emission inventories, *Environ. Sci. Technol.*, 46, 3528-3535, 2012.

305 Freyer, H. D.: Seasonal variation of ¹⁵N/¹⁴N ratios in atmospheric nitrate species, *Tellus B*, 43, 30-44, 1991.

306 Freyer, H. D., Kley, D., Volz - Thomas, A., and Kobel, K.: On the interaction of isotopic exchange processes with
307 photochemical reactions in atmospheric oxides of nitrogen, *J. Geophys. Res. Atmos.*, 98, 14791-14796, 1993.

308 Geng, L., Alexander, B., Cole-Dai, J., Steig, E. J., Savarino, J., Sofen, E. D., and Schauer, A. J.: Nitrogen isotopes in ice core
309 nitrate linked to anthropogenic atmospheric acidity change, *Proc. Natl. Acad. Sci. USA*, 111, 5808-5812, 2014.

310 Goodman, A. L., Underwood, G. M., and Grassian, V. H.: Heterogeneous reaction of NO₂: Characterization of gas-phase

311 and adsorbed products from the reaction, $2\text{NO}_2(\text{g}) + \text{H}_2\text{O}(\text{a}) \rightarrow \text{HONO}(\text{g}) + \text{HNO}_3(\text{a})$ on hydrated silica particles, *J.*
312 *Phys. Chem. A*, 103, 7217-7223, 1999.

313 Guha, T., Lin, C. T., Bhattacharya, S. K., Mahajan, A. S., Ou-Yang, C.-F., Lan, Y.-P., Hsu, S. C., and Liang, M.-C.: Isotopic
314 ratios of nitrate in aerosol samples from Mt. Lulin, a high-altitude station in Central Taiwan, *Atmos. Environ.*, 154,
315 53-69, 2017.

316 Hastings, M. G., Casciotti, K. L., and Elliott, E. M.: Stable isotopes as tracers of anthropogenic nitrogen sources, deposition,
317 and impacts, *Elements*, 9, 339-344, 2013.

318 He, P., Alexander, B., Geng, L., Chi, X., Fan, S., Zhan, H., Kang, H., Zheng, G., Cheng, Y., Su, H., Liu, C., and Xie, Z.:
319 Isotopic constraints on heterogeneous sulfate production in Beijing haze, *Atmos. Chem. Phys.*, 18, 5515-5528, 2018.

320 Hoering, T.: The isotopic composition of the ammonia and the nitrate ion in rain, *Geochim. Cosmochim. Acta*, 12, 97-102,
321 1957.

322 Ishino, S., Hattori, S., Savarino, J., Jourdain, B., Preunkert, S., Legrand, M., Caillon, N., Barbero, A., Kuribayashi, K., and
323 Yoshida, N.: Seasonal variations of triple oxygen isotopic compositions of atmospheric sulfate, nitrate, and ozone at
324 Dumont d'Urville, coastal Antarctica, *Atmos. Chem. Phys.*, 17, 3713-3727, 2017.

325 Kaiser, J., Hastings, M. G., Houlton, B. Z., Röckmann, T., and Sigman, D. M.: Triple oxygen isotope analysis of nitrate using
326 the denitrifier method and thermal decomposition of N_2O , *Anal. Chem.*, 79, 599-607, 2007.

327 Kanaya, Y., Cao, R., Akimoto, H., Fukuda, M., Komazaki, Y., Yokouchi, Y., Koike, M., Tanimoto, H., Takegawa, N., and
328 Kondo, Y.: Urban photochemistry in central Tokyo: 1. Observed and modeled OH and HO₂ radical concentrations
329 during the winter and summer of 2004, *J. Geophys. Res.*, 112, 2007.

330 Kunasek, S. A., Alexander, B., Steig, E. J., Hastings, M. G., Gleason, D. J., and Jarvis, J. C.: Measurements and modeling of
331 $\Delta^{17}\text{O}$ of nitrate in snowpits from Summit, Greenland, *J. Geophys. Res.*, 113, 2008.

332 Li, H., Zhu, T., Zhao, D., Zhang, Z., and Chen, Z.: Kinetics and mechanisms of heterogeneous reaction of NO_2 on CaCO_3
333 surfaces under dry and wet conditions, *Atmos. Chem. Phys.*, 10, 463-474, 2010.

334 Li, Z., Hu, R., Xie, P., Wang, H., Lu, K., and Wang, D.: Intercomparison of in situ CRDS and CEAS for measurements of
335 atmospheric N_2O_5 in Beijing, China, *Sci. Total Environ.*, 613, 131-139, 2018.

336 Liang, J., Horowitz, L. W., Jacob, D. J., Wang, Y., Fiore, A. M., Logan, J. A., Gardner, G. M., and Munger, J. W.: Seasonal
337 budgets of reactive nitrogen species and ozone over the United States, and export fluxes to the global atmosphere, *J.*
338 *Geophys. Res. Atmos.*, 103, 13435-13450, 1998.

339 Lin, J.-T.: Satellite constraint for emissions of nitrogen oxides from anthropogenic, lightning and soil sources over East
340 China on a high-resolution grid, *Atmos. Chem. Phys.*, 12, 2881-2898, 2012.

341 Lin, W., Xu, X., Ge, B., and Liu, X.: Gaseous pollutants in Beijing urban area during the heating period 2007–2008:

342 variability, sources, meteorological, and chemical impacts, *Atmos. Chem. Phys.*, 11, 8157-8170, 2011.

343 Liu, Z., Wang, Y., Gu, D., Zhao, C., Huey, L., Stickel, R., Liao, J., Shao, M., Zhu, T., and Zeng, L.: Summertime
344 photochemistry during CAREBeijing-2007: ROx budgets and O₃ formation, *Atmos. Chem. Phys.*, 12, 7737-7752, 2012.

345 Michalski, G., Scott, Z., Kabling, M., and Thiemens, M. H.: First measurements and modeling of $\Delta^{17}\text{O}$ in atmospheric
346 nitrate, *Geophys. Res. Lett.*, 30, 2003.

347 Mihelcic, D., Holland, F., Hofzumahaus, A., Hoppe, L., Konrad, S., M \ddot{u} sgen, P., P \ddot{a} tz, H. W., Sch \ddot{a} fer, H. J., Schmitz, T., and
348 Volz - Thomas, A.: Peroxy radicals during BERLIOZ at Pabstthum: Measurements, radical budgets and ozone
349 production, *J. Geophys. Res.*, 108, 2003.

350 Morin, S., Savarino, J., Bekki, S., Cavender, A., Shepson, P. B., and Bottenheim, J. W.: Major influence of BrO on the NOx
351 and nitrate budgets in the Arctic spring, inferred from $\Delta^{17}\text{O}(\text{NO}_3^-)$ measurements during ozone depletion events,
352 *Environ. Chem.*, 4, 238, 2007a.

353 Morin, S., Savarino, J., Bekki, S., Gong, S., and Bottenheim, J. W.: Signature of Arctic surface ozone depletion events in the
354 isotope anomaly ($\Delta^{17}\text{O}$) of atmospheric nitrate, *Atmos. Chem. Phys.*, 7, 1451-1469, 2007b.

355 Morin, S., Savarino, J., Frey, M. M., Yan, N., Bekki, S., Bottenheim, J. W., and Martins, J. M.: Tracing the origin and fate of
356 NOx in the Arctic atmosphere using stable isotopes in nitrate, *Science*, 322, 730-732, 2008.

357 Morin, S., Savarino, J., Frey, M. M., Domine, F., Jacobi, H. W., Kaleschke, L., and Martins, J. M.: Comprehensive isotopic
358 composition of atmospheric nitrate in the Atlantic Ocean boundary layer from 65 S to 79 N, *J. Geophys. Res. Atmos.*,
359 114, 2009.

360 Morin, S., Sander, R., and Savarino, J.: Simulation of the diurnal variations of the oxygen isotope anomaly ($\Delta^{17}\text{O}$) of reactive
361 atmospheric species, *Atmos. Chem. Phys.*, 11, 3653-3671, 2011.

362 Pathak, R. K., Wu, W. S., and Wang, T.: Summertime PM_{2.5} ionic species in four major cities of China: nitrate formation in
363 an ammonia-deficient atmosphere, *Atmos. Chem. Phys.*, 9, 1711-1722, 2009.

364 Pathak, R. K., Wang, T., and Wu, W. S.: Nighttime enhancement of PM_{2.5} nitrate in ammonia-poor atmospheric conditions
365 in Beijing and Shanghai: plausible contributions of heterogeneous hydrolysis of N₂O₅ and HNO₃ partitioning, *Atmos.*
366 *Environ.*, 45, 1183-1191, 2011.

367 Patris, N., Cliff, S. S., Quinn, P. K., Kasem, M., and Thiemens, M. H.: Isotopic analysis of aerosol sulfate and nitrate during
368 ITCT - 2k2: Determination of different formation pathways as a function of particle size, *J. Geophys. Res. Atmos.*, 112,
369 2007.

370 Rao, Z., Chen, Z., Liang, H., Huang, L., and Huang, D.: Carbonyl compounds over urban Beijing: Concentrations on haze
371 and non-haze days and effects on radical chemistry, *Atmos. Environ.*, 124, 207-216, 2016.

372 Savarino, J., and Thiemens, M. H.: Analytical procedure to determine both $\delta^{18}\text{O}$ and $\delta^{17}\text{O}$ of H₂O₂ in natural water and first

373 measurements, *Atmos. Environ.*, 33, 3683-3690, 1999.

374 Savarino, J., Kaiser, J., Morin, S., Sigman, D. M., and Thiemens, M. H.: Nitrogen and oxygen isotopic constraints on the
375 origin of atmospheric nitrate in coastal Antarctica, *Atmos. Chem. Phys.*, 7, 1925-1945, 2007.

376 Savarino, J., Bhattacharya, S. K., Morin, S., Baroni, M., and Doussin, J.-F.: The NO + O₃ reaction: A triple oxygen isotope
377 perspective on the reaction dynamics and atmospheric implications for the transfer of the ozone isotope anomaly, *J.*
378 *Chem. Phys.*, 128, 194303, 2008.

379 Savarino, J., Morin, S., Erbland, J., Grannec, F., Patey, M. D., Vicars, W., Alexander, B., and Achterberg, E. P.: Isotopic
380 composition of atmospheric nitrate in a tropical marine boundary layer, *P. Natl. Acad. Sci. USA*, 110, 17668-17673,
381 2013.

382 Sofen, E. D., Alexander, B., Steig, E. J., Thiemens, M. H., Kunasek, S. A., Amos, H. M., Schauer, A. J., Hastings, M. G.,
383 Bautista, J., and Jackson, T. L.: WAIS Divide ice core suggests sustained changes in the atmospheric formation
384 pathways of sulfate and nitrate since the 19th century in the extratropical Southern Hemisphere, *Atmos. Chem. Phys.*,
385 14, 5749-5769, 2014.

386 Su, X., Tie, X., Li, G., Cao, J., Huang, R., Feng, T., Long, X., and Xu, R.: Effect of hydrolysis of N₂O₅ on nitrate and
387 ammonium formation in Beijing China: WRF-Chem model simulation, *Sci. Total Environ.*, 579, 221-229, 2017.

388 Sun, Y., Zhuang, G., Tang, A., Wang, Y., and An, Z.: Chemical characteristics of PM_{2.5} and PM₁₀ in haze-fog episodes in
389 Beijing, *Environ. Sci. Technol.*, 40, 3148-3155, 2006.

390 Tong, S., Hou, S., Zhang, Y., Chu, B., Liu, Y., He, H., Zhao, P., and Ge, M.: Comparisons of measured nitrous acid (HONO)
391 concentrations in a pollution period at urban and suburban Beijing, in autumn of 2014, *Sci. China Chem.*, 58,
392 1393-1402, 2015.

393 Vicars, W. C., Morin, S., Savarino, J., Wagner, N. L., Erbland, J., Vince, E., Martins, J. M. F., Lerner, B. M., Quinn, P. K.,
394 and Coffman, D. J.: Spatial and diurnal variability in reactive nitrogen oxide chemistry as reflected in the isotopic
395 composition of atmospheric nitrate: Results from the CalNex 2010 field study, *J. Geophys. Res. Atmos.*, 118, 2013.

396 Vicars, W. C., and Savarino, J.: Quantitative constraints on the 17O-excess ($\Delta^{17}\text{O}$) signature of surface ozone: Ambient
397 measurements from 50°N to 50°S using the nitrite-coated filter technique, *Geochim. Cosmochim. Acta*, 135, 270-287,
398 2014.

399 Walters, W. W., Simonini, D. S., and Michalski, G.: Nitrogen isotope exchange between NO and NO₂ and its implications for
400 $\delta^{15}\text{N}$ variations in tropospheric NO_x and atmospheric nitrate, *Geophys. Res. Lett.*, 43, 440-448, 2016.

401 Wang, D., Hu, R., Xie, P., Liu, J., Liu, W., Qin, M., Ling, L., Zeng, Y., Chen, H., Xing, X., Zhu, G., Wu, J., Duan, J., Lu, X.,
402 and Shen, L.: Diode laser cavity ring-down spectroscopy for in situ measurement of NO₃ radical in ambient air, *J. Quant.*
403 *Spectrosc. Radiat. Transf.*, 166, 23-29, 2015.

404 Wang, H., Chen, J., and Lu, K.: Development of a portable cavity-enhanced absorption spectrometer for the measurement of
405 ambient NO_3 and N_2O_5 : experimental setup, lab characterizations, and field applications in a polluted urban
406 environment, *Atmos. Meas. Tech.*, 10, 1465, 2017a.

407 Wang, H., Lu, K., Chen, X., Zhu, Q., Chen, Q., Guo, S., Jiang, M., Li, X., Shang, D., and Tan, Z.: High N_2O_5 concentrations
408 observed in urban Beijing: Implications of a large nitrate formation pathway, *Environ. Sci. Technol. Lett.*, 4, 416-420,
409 2017b.

410 Wang, H., Lu, K., Tan, Z., Sun, K., Li, X., Hu, M., Shao, M., Zeng, L., Zhu, T., and Zhang, Y.: Model simulation of NO_3 ,
411 N_2O_5 and ClNO_2 at a rural site in Beijing during CAREBeijing-2006, *Atmos. Res.*, 196, 97-107, 2017c.

412 Wang, H., Lu, K., Chen, X., Zhu, Q., Wu, Z., Wu, Y., and Sun, K.: Large particulate nitrate formation from N_2O_5 uptake in a
413 chemically reactive layer aloft during wintertime in Beijing, *Atmos. Chem. Phys. Discuss.*, 1-27, 2018a.

414 Wang, H., Lu, K., Guo, S., Wu, Z., Shang, D., Tan, Z., Wang, Y., Le Breton, M., Zhu, W., Lou, S., Tang, M., Wu, Y., Zheng,
415 J., Zeng, L., Hallquist, M., Hu, M., and Zhang, Y.: Efficient N_2O_5 Uptake and NO_3 Oxidation in the Outflow of Urban
416 Beijing, *Atmos. Chem. Phys. Discuss.*, 1-27, 2018b.

417 Wang, J., Zhang, X., Guo, J., Wang, Z., and Zhang, M.: Observation of nitrous acid (HONO) in Beijing, China: Seasonal
418 variation, nocturnal formation and daytime budget, *Sci. Total Environ.*, 587, 350-359, 2017d.

419 Wang, S., Zhang, Q., Streets, D. G., He, K., Martin, R. V., Lamsal, L. N., Chen, D., Lei, Y., and Lu, Z.: Growth in NO_x
420 emissions from power plants in China: bottom-up estimates and satellite observations, *Atmos. Chem. Phys.*, 12,
421 4429-4447, 2012.

422 Wang, Y., Zhou, L., Wang, M., and Zheng, X.: Trends of atmospheric methane in Beijing, *Chemosphere*, 3, 65-71, 2001.

423 Wen, L., Chen, J., Yang, L., Wang, X., Xu, C., Sui, X., Yao, L., Zhu, Y., Zhang, J., and Zhu, T.: Enhanced formation of fine
424 particulate nitrate at a rural site on the North China Plain in summer: The important roles of ammonia and ozone, *Atmos.*
425 *Environ.*, 101, 294-302, 2015.

426 Wu, R., Li, J., Hao, Y., Li, Y., Zeng, L., and Xie, S.: Evolution process and sources of ambient volatile organic compounds
427 during a severe haze event in Beijing, China, *Sci. Total Environ.*, 560, 62-72, 2016.

428 Xiao, H., Xie, L., Long, A., Ye, F., Pan, Y., Li, D., Long, Z., Chen, L., Xiao, H., and Liu, C.: Use of isotopic compositions of
429 nitrate in TSP to identify sources and chemistry in South China Sea, *Atmos. Environ.*, 109, 70-78, 2015.

430 Xu, X., Zhao, W., Zhang, Q., Wang, S., Fang, B., Chen, W., Venables, D. S., Wang, X., Pu, W., and Wang, X.: Optical
431 properties of atmospheric fine particles near Beijing during the HOPE-J3 A campaign, *Atmos. Chem. Phys.*, 16,
432 6421-6439, 2016.

433 Ye, P., Xie, Z., Yu, J., and Kang, H.: Spatial distribution of methanesulphonic acid in the Arctic aerosol collected during the
434 Chinese Arctic Research Expedition, *Atmosphere*, 6, 699-712, 2015.

435 Yu, Z., and Elliott, E. M.: Novel Method for Nitrogen Isotopic Analysis of Soil-Emitted Nitric Oxide, *Environ. Sci. Technol.*,
 436 2017.

437 Zhang, J., Chen, Z., Lu, Y., Gui, H., Liu, J., Liu, W., Wang, J., Yu, T., Cheng, Y., and Chen, Y.: Characteristics of aerosol size
 438 distribution and vertical backscattering coefficient profile during 2014 APEC in Beijing, *Atmos. Environ.*, 148, 30-41,
 439 2017.

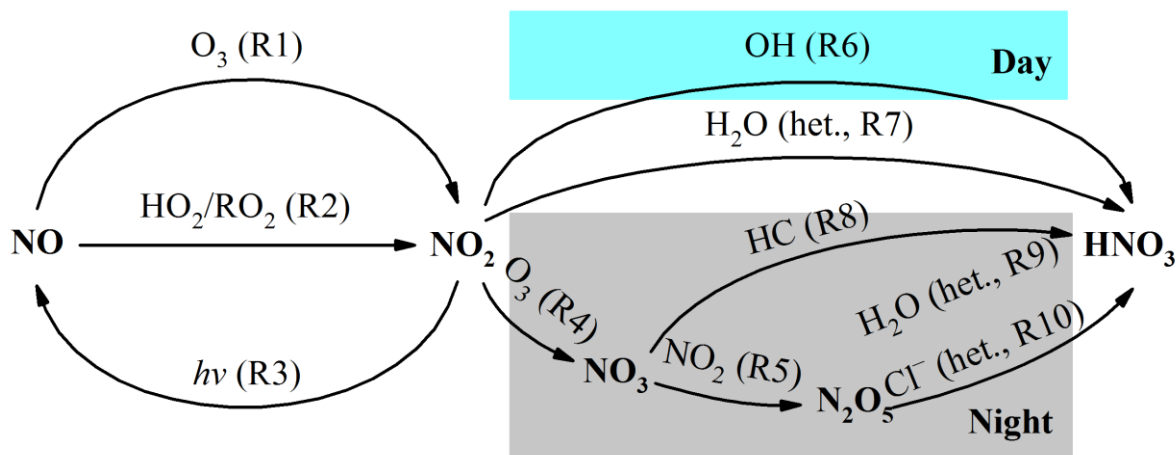
440 Zhang, Q., Streets, D. G., He, K., Wang, Y., Richter, A., Burrows, J. P., Uno, I., Jang, C. J., Chen, D., Yao, Z., and Lei, Y.:
 441 NO_x emission trends for China, 1995–2004: The view from the ground and the view from space, *J. Geophys. Res.*, 112,
 442 2007.

443 Zhang, Y., Liu, X., Fangmeier, A., Goulding, K. T. W., and Zhang, F.: Nitrogen inputs and isotopes in precipitation in the
 444 North China Plain, *Atmos. Environ.*, 42, 1436-1448, 2008.

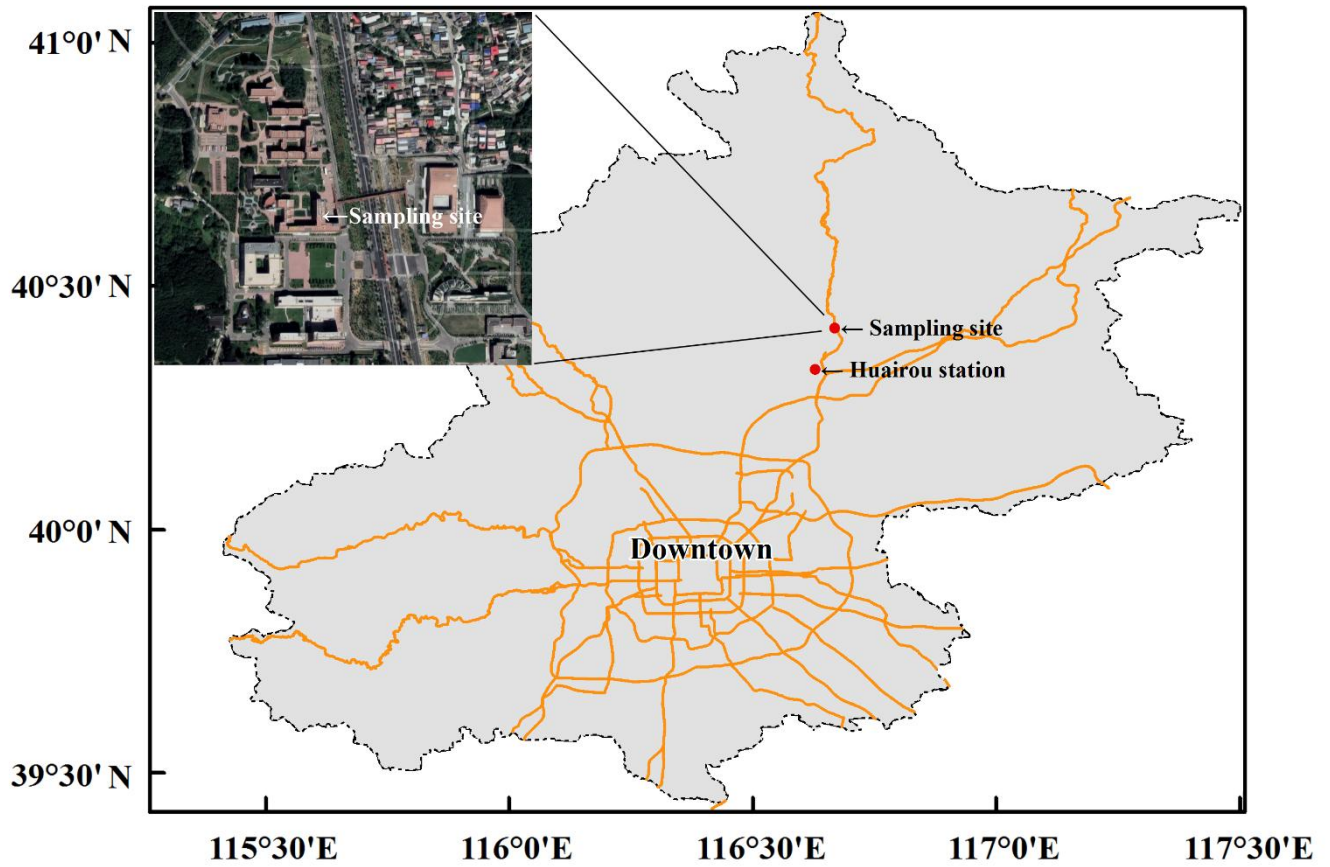
445 Zheng, B., Zhang, Q., Zhang, Y., He, K., Wang, K., Zheng, G., Duan, F., Ma, Y., and Kimoto, T.: Heterogeneous chemistry: a
 446 mechanism missing in current models to explain secondary inorganic aerosol formation during the January 2013 haze
 447 episode in North China, *Atmos. Chem. Phys.*, 15, 2031-2049, 2015a.

448 Zheng, G., Duan, F., Su, H., Ma, Y., Cheng, Y., Zheng, B., Zhang, Q., Huang, T., Kimoto, T., and Chang, D.: Exploring the
 449 severe winter haze in Beijing: the impact of synoptic weather, regional transport and heterogeneous reactions, *Atmos.*
 450 *Chem. Phys.*, 15, 2969-2983, 2015b.

451 **Figures and Tables**



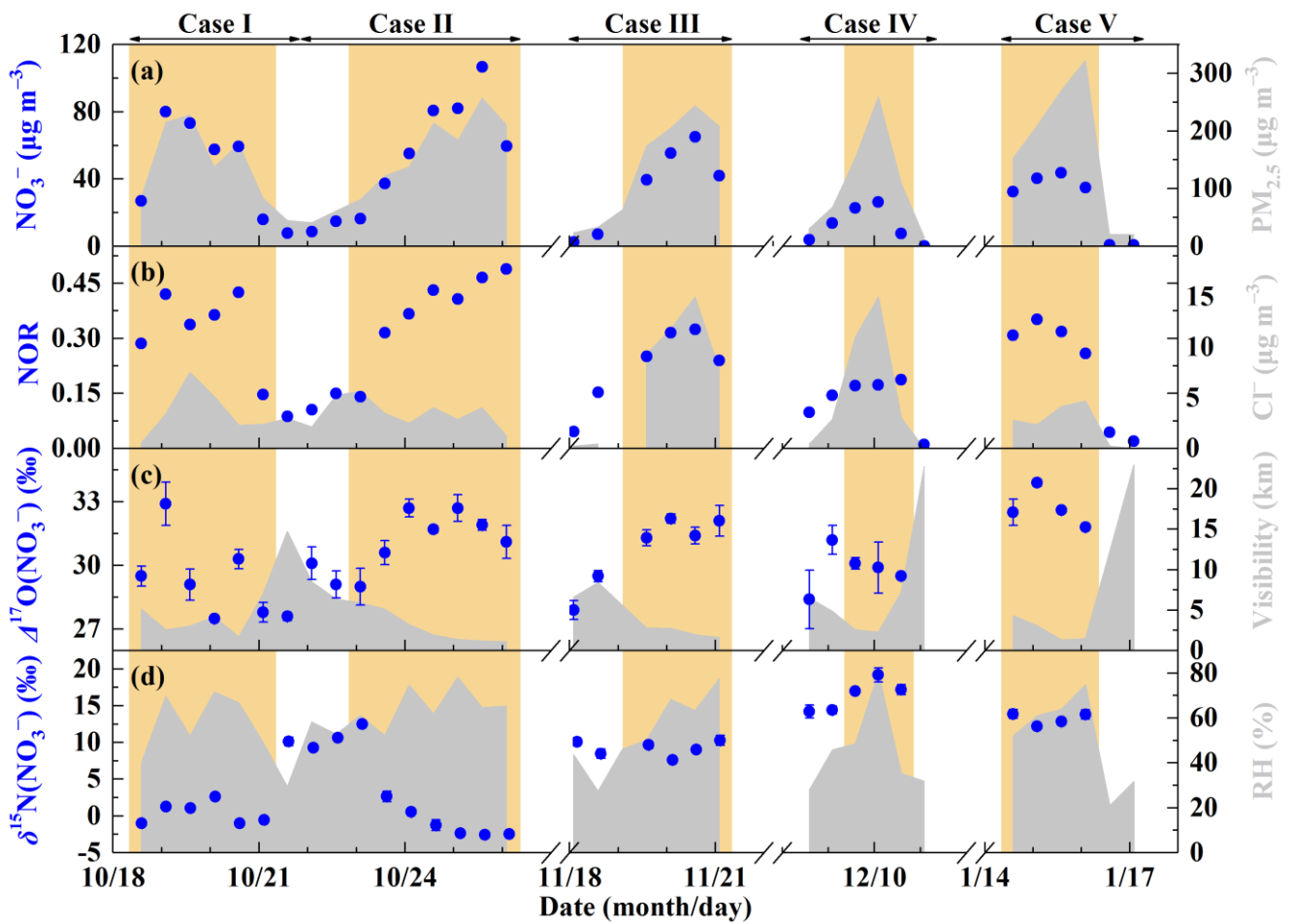
452
 453 **Figure 1.** Simplified schematic of the main nitrate formation pathways in urban air. “het.” means heterogeneous reactions on
 454 aerosols.



455

456 **Figure 2.** A brief map of sampling site in Beijing. The map scale of base map is 1:1250000. Huairou station is set by Beijing

457 Municipal Environmental Monitoring Center, where hourly $PM_{2.5}$, SO_2 , CO, NO_2 and O_3 were observed.



458

459

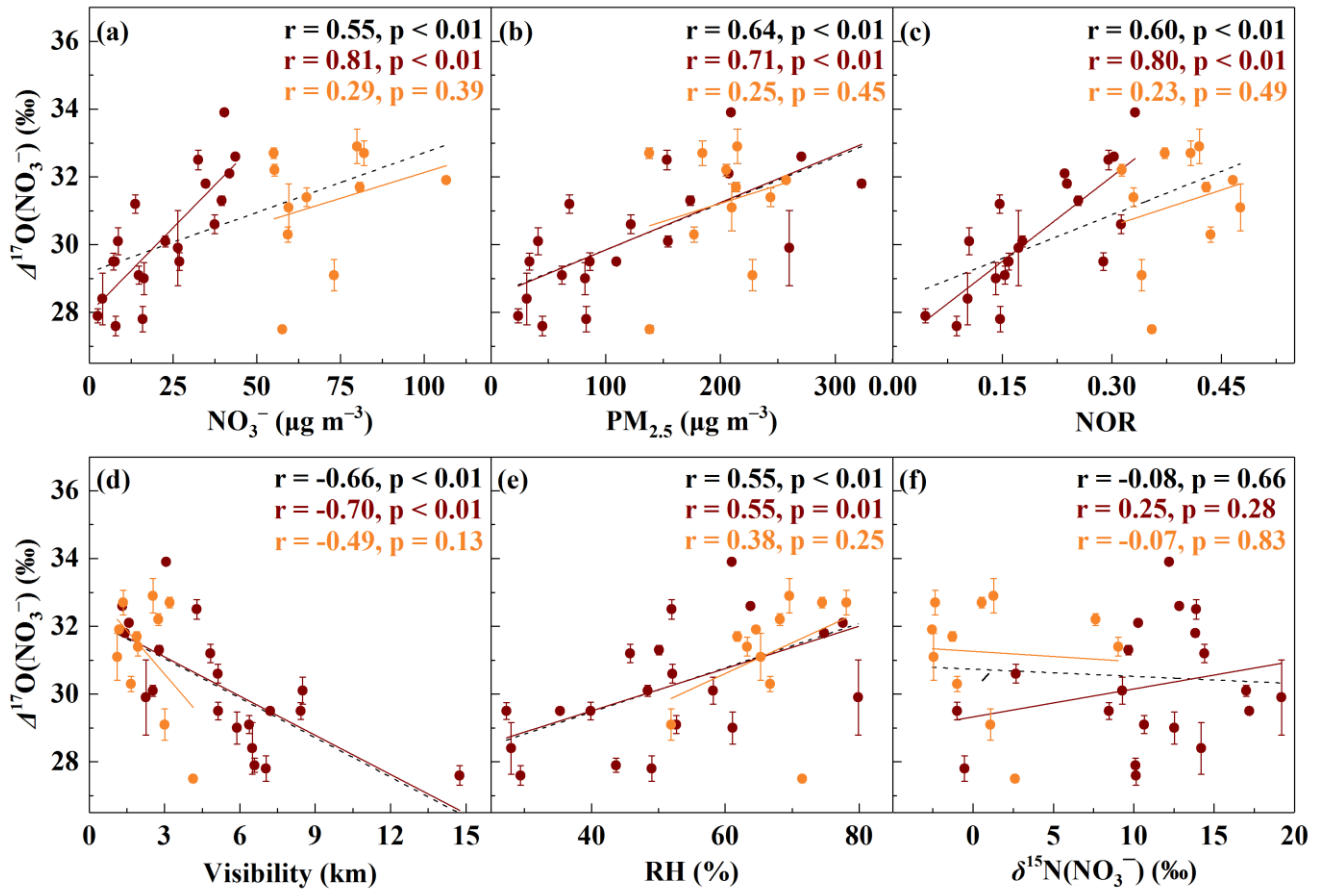
460

461

462

463

Figure 3. General characteristics of haze events in Beijing (October 2014 – January 2015). (a) Time series of $\text{PM}_{2.5}$ and NO_3^- concentrations. (b) Time series of nitrogen oxidation ratio (NOR, which equals to NO_3^- molar concentration divided by the sum of NO_3^- and NO_2 molar concentration) and Cl^- concentrations. (c) Time series of $\Delta^{17}\text{O}(\text{NO}_3^-)$ and visibility. (d) Time series of $\delta^{15}\text{N}(\text{NO}_3^-)$ and relative humidity (RH). The error bars in (c) and (d) are $\pm 1\sigma$ of replicate measurements ($n = 3$) of each sample. The khaki shaded area indicates polluted days (PD, $\text{PM}_{2.5} \geq 75 \mu\text{g m}^{-3}$).



464

465

466

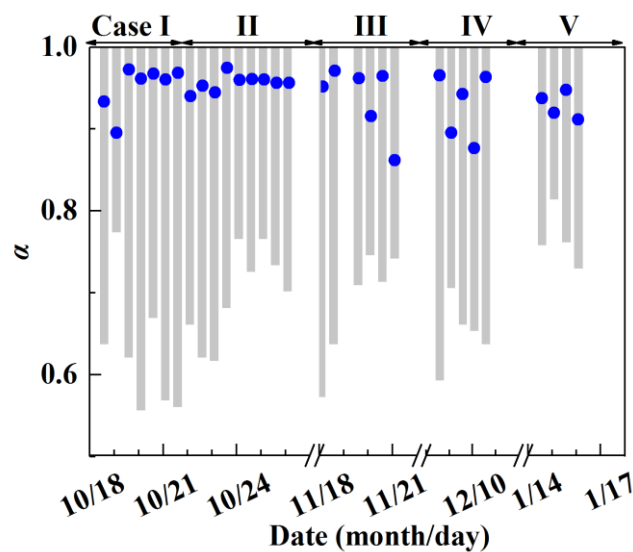
467

468

469

470

Figure 4. Relationships between $\Delta^{17}\text{O}(\text{NO}_3^-)$ and other parameters. The relationship between $\Delta^{17}\text{O}(\text{NO}_3^-)$ and NO_3^- concentrations (a), $\text{PM}_{2.5}$ concentrations (b), nitrogen oxidation ratio (NOR, c), visibility (d), relative humidity (RH, e) and $\delta^{15}\text{N}(\text{NO}_3^-)$ (f). The dark red dots are samples with $\text{NO}_3^- < 50 \mu\text{g m}^{-3}$ and the orange dots are samples with $\text{NO}_3^- > 50 \mu\text{g m}^{-3}$. The black dash lines are linear least-squares fitting lines for all samples, the dark red solid lines are linear least-squares fitting lines for samples with $\text{NO}_3^- < 50 \mu\text{g m}^{-3}$ and the orange solid lines are linear least-squares fitting lines for samples with $\text{NO}_3^- > 50 \mu\text{g m}^{-3}$. The error bars are $\pm 1\sigma$ of replicate measurements of each sample.

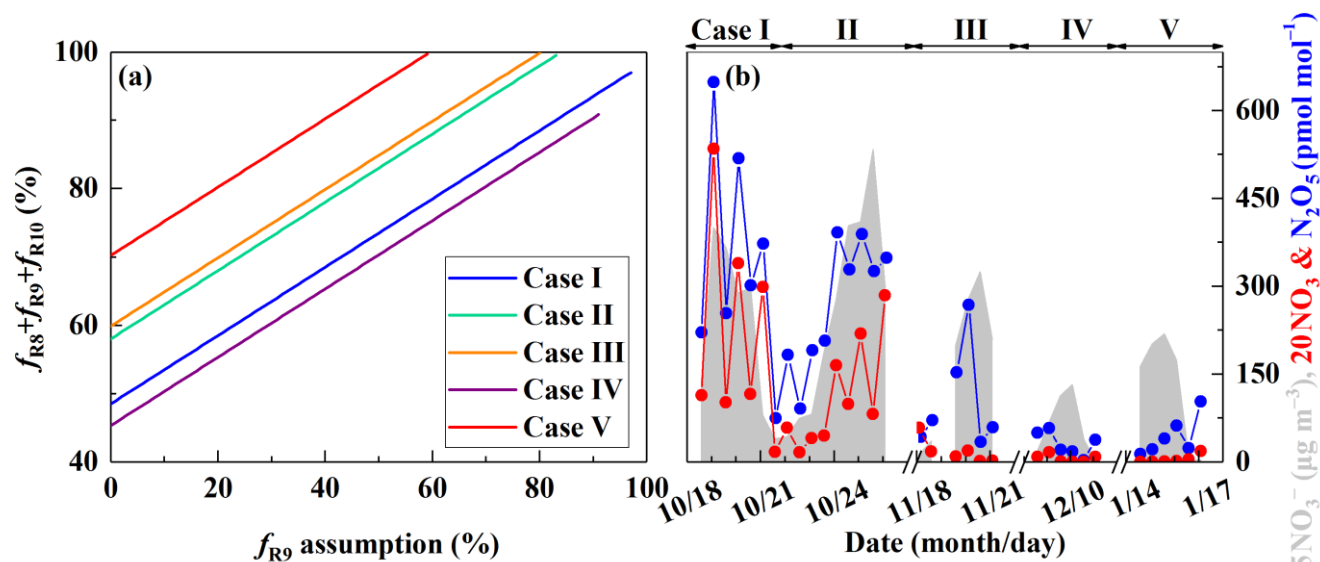


471

472

Figure 5. Estimate of the proportion of O_3 oxidation in NO_x cycling, α . The gray column represents possible α range

473 determined by $\Delta^{17}\text{O}(\text{NO}_3^-)$. The blue dot represents specific α value calculated by Eq. (3).



474
 475 **Figure 6.** Estimate of the nocturnal formation pathways. The estimated relative importance of nocturnal formation pathways
 476 ($f_{\text{R8}} + f_{\text{R9}} + f_{\text{R10}}$) during PD of each case on the basis of observed $\Delta^{17}\text{O}(\text{NO}_3^-)$ (See Sect. 2.3, a) and the simulated mixing
 477 ratios of N_2O_5 and NO_3 radical by MCM (b). R8, R9 and R10 in (a) represents $\text{NO}_3 + \text{HC}$, $\text{N}_2\text{O}_5 + \text{H}_2\text{O}$ and $\text{N}_2\text{O}_5 + \text{Cl}^-$
 478 pathway, respectively.

479 **Table 1.** Isotope assumptions of different nitrate formation pathways.

No.	Reaction	$\Delta^{17}\text{O}$ of product		Reference
		Expression	Value (‰) ^a	
R1	$\text{NO} + \text{O}_3 \rightarrow \text{NO}_2 + \text{O}_2$	$\Delta^{17}\text{O}(\text{NO}_2) = 1.18 \times \Delta^{17}\text{O}(\text{O}_3) + 6.6 \text{‰}$	37	(Savarino et al., 2008)
R2	$\text{NO} + \text{HO}_2/\text{RO}_2 \rightarrow \text{NO}_2 + \text{OH}/\text{RO}$	$\Delta^{17}\text{O}(\text{NO}_2) = 0.0$	0.0	(Sofen et al., 2014)
R4	$\text{NO}_2 + \text{O}_3 \rightarrow \text{NO}_3 + \text{O}_2$	$\Delta^{17}\text{O}(\text{NO}_3) =$ $\frac{2}{3}\Delta^{17}\text{O}(\text{NO}_2) + \frac{1}{3}(1.23 \times \Delta^{17}\text{O}(\text{O}_3) + 9.0 \text{‰})$	$25\alpha + 14$	(Berhanu et al., 2012)
R5	$\text{NO}_2 + \text{NO}_3 \rightarrow \text{N}_2\text{O}_5$	$\Delta^{17}\text{O}(\text{N}_2\text{O}_5) = \frac{2}{5}\Delta^{17}\text{O}(\text{NO}_2) + \frac{3}{5}\Delta^{17}\text{O}(\text{NO}_3)$	$30\alpha + 8$	(Sofen et al., 2014)
R6	$\text{NO}_2 + \text{OH} \rightarrow \text{HNO}_3$	$\Delta^{17}\text{O}(\text{NO}_3^-) = \frac{2}{3}\Delta^{17}\text{O}(\text{NO}_2)$	25α	(Sofen et al., 2014)
R7	$2\text{NO}_2 + \text{H}_2\text{O} \rightarrow \text{HNO}_3 + \text{HNO}_2$	$\Delta^{17}\text{O}(\text{NO}_3^-) = \frac{2}{3}\Delta^{17}\text{O}(\text{NO}_2)$	25α	^b
R8	$\text{NO}_3 + \text{HC} \rightarrow \text{HNO}_3 + \text{products}$	$\Delta^{17}\text{O}(\text{NO}_3^-) = \Delta^{17}\text{O}(\text{NO}_3)$	$25\alpha + 14$	(Sofen et al., 2014)
R9	$\text{N}_2\text{O}_5 + \text{H}_2\text{O} \rightarrow 2\text{HNO}_3$	$\Delta^{17}\text{O}(\text{NO}_3^-) = \frac{5}{6}\Delta^{17}\text{O}(\text{N}_2\text{O}_5)$	$25\alpha + 7$	(Sofen et al., 2014)
R10	$\text{N}_2\text{O}_5 + \text{Cl}^- \rightarrow \text{HNO}_3 + \text{ClNO}_2$	$\Delta^{17}\text{O}(\text{NO}_3^-) = \Delta^{17}\text{O}(\text{NO}_3)$	$25\alpha + 14$	^c

480 ^a The values are calculated on assumptions that bulk $\Delta^{17}\text{O}(\text{O}_3) = 26 \text{‰}$ (Vicars and Savarino, 2014; Ishino et al., 2017) and

481 $\Delta^{17}\text{O}(\text{HO}_2/\text{RO}_2) = 0 \text{‰}$. $\Delta^{17}\text{O}(\text{RO}_2)$ is equal to 0‰ in the troposphere (Morin et al., 2011), in contrast, observations suggest

482 $\Delta^{17}\text{O}(\text{HO}_2) = 1 - 2 \text{ ‰}$ (Savarino and Thiemens, 1999). However, the difference in calculated $\Delta^{17}\text{O}(\text{NO}_3^-)$ between assuming
 483 $\Delta^{17}\text{O}(\text{HO}_2) = 0 \text{ ‰}$ and $\Delta^{17}\text{O}(\text{HO}_2) = 2 \text{ ‰}$ is negligible in this study ($< 0.1 \text{ ‰}$). And the assumption that $\Delta^{17}\text{O}(\text{HO}_2) = 0 \text{ ‰}$
 484 simplifies calculations and is also consistent with previous studies (Michalski et al., 2003; Alexander et al., 2009; Morin et
 485 al., 2008; Kunasek et al., 2008; Sofen et al., 2014). α is the proportion of O_3 oxidation in NO_2 production rate, calculated by
 486 Eq. (3).

487 ^b Previous studies suggest that in R7 one oxygen atom of NO_3^- is from H_2O and the other two are from NO_2 (Li et al., 2010;
 488 Cheung et al., 2000; Goodman et al., 1999), which will result in $\Delta^{17}\text{O}(\text{NO}_3^-) = 2/3\Delta^{17}\text{O}(\text{NO}_2)$.

489 ^c R4 and R5 suggest that the central oxygen atom of N_2O_5 ($\text{O}_2\text{N-O-NO}_2$) is from NO_3 radical (O-NO_2) with $\Delta^{17}\text{O} (\text{‰}) =$
 490 $1.23 \times \Delta^{17}\text{O}(\text{O}_3) + 9.0 \text{ ‰}$. R10 is suggested to occur via $\text{O}_2\text{N-O-NO}_2 (\text{aq}) \leftrightarrow \text{NO}_2^+ + \text{NO}_3^-$ and the following $\text{NO}_2^+ + \text{Cl}^- \rightarrow$
 491 ClNO_2 (Bertram and Thornton, 2009), so $\Delta^{17}\text{O}(\text{NO}_3^-) = 1/3(1.23 \times \Delta^{17}\text{O}(\text{O}_3) + 9.0 \text{ ‰}) + 2/3\Delta^{17}\text{O}(\text{NO}_2) = \Delta^{17}\text{O}(\text{NO}_3)$.

492 **Table 2.** Reaction expressions for different NO_2 production pathways.

No.	Reaction	Rate expression	Rate constant ($\text{cm}^3 \text{ molecule}^{-1} \text{ s}^{-1}$)	Reference
R1	$\text{NO} + \text{O}_3 \rightarrow \text{NO}_2 + \text{O}_2$	$k_{\text{R1}}[\text{NO}][\text{O}_3]$	$k_{\text{R1}} = 3.0 \times 10^{-12} \times e^{(-1500/T)}$	(Burkholder et al., 2015)
R2a	$\text{NO} + \text{HO}_2 \rightarrow \text{NO}_2 + \text{OH}$	$k_{2\text{Ra}}[\text{NO}][\text{HO}_2]$	$k_{2\text{Ra}} = 3.3 \times 10^{-12} \times e^{(270/T)}$	(Burkholder et al., 2015)
R2b	$\text{NO} + \text{RO}_2 \rightarrow \text{NO}_2 + \text{RO}$	$k_{2\text{Rb}}[\text{NO}][\text{RO}_2]$	$k_{2\text{Rb}} = k_{2\text{Ra}}$	(Burkholder et al., 2015; Kunasek et al., 2008)

493 **Table 3.** Atmospheric $\Delta^{17}\text{O}(\text{NO}_3^-)$ in aerosols obtained from the literature and this study.

Sample location	Sample period	Collection interval	$\Delta^{17}\text{O} (\text{‰})$ range	Reference
Huairou, Beijing (40.41 °N, 116.68 °E)	October 2014 – January 2015	12 h	27.5 – 33.9 (30.6 ± 1.8)	This study
Trinidad Head, California (41.0 °N, 124.2 °W)	April – May 2002	1 – 4 days	20.1 – 27.5	(Patris et al., 2007)
La Jolla, California (32.7 °N, 117.2 °W)	March 1997 – April 1998	3 days	20 – 30.8	(Michalski et al., 2003)
Mt. Lulin, Taiwan (23.5 °N, 120.9 °E)	January – December 2010	1 day	2.7 – 31.4 (17 ± 7)	(Guha et al., 2017)
Cape Verde Island (16.9 °N, 24.9 °W)	July 2007 – May 2008	2 – 3 days	25.5 – 31.3	(Savarino et al., 2013)
Cruise in costal California (32.8 °N – 38.6 °N)	May – June 2010	2 – 22 h	19.0 – 29.2 (24.1 ± 2.2)	(Vicars et al., 2013)

Cruise from 65 °S to 79 °N	September – October 2006	1 – 4 days	Non-polar:	(Morin et al., 2009)
	April – May 2007		24 – 33	
	February – April 2006		Polar: 35 ± 2	
Alert, Nunavut (82.5 °N, 62.3 °W)	March – May 2004	3 – 4 days	29 – 35 (32.7 ± 1.8)	(Morin et al., 2007b)
Barrow, Alaska (71.3 °N, 156.9 °W)	March 2005	1 day	26 – 36	(Morin et al., 2007a)
Dumont d'Urville, Antarctic (66.7 °S, 140.0 °E)	January – December 2001	10 – 15 days	20.0 – 43.1	(Savarino et al., 2007)
Dumont d'Urville, Antarctic (66.7 °S, 140.0 °E)	January 2011 – January 2012	7 days	23.0 – 41.9	(Ishino et al., 2017)

494 **Table 4** The possible range of fractional contribution of different nitrate formation pathways during PD of each case
495 estimated on the basis of observed $\Delta^{17}\text{O}(\text{NO}_3^-)$ ^a.

PD of Case	f_{R9} assumption (%)	$f_{R8} + f_{R9} + f_{R10}$ (%)	$f_{R8} + f_{R10}$ (%)	$f_{R6} + f_{R7}$ (%)
I	0 – 97	49 – 97	0 – 49	3 – 51
II	0 – 83	58 – 100	17 – 58	0 – 42
III	0 – 80	60 – 100	20 – 60	0 – 40
IV	0 – 90	45 – 90	0 – 45	10 – 55
V	0 – 59	70 – 100	41 – 70	0 – 30
Average	0 – 82	56 – 97	16 – 56	3 – 44

496 ^a R6, R7, R8, R9 and R10 is respectively $\text{NO}_2 + \text{OH}$, $\text{NO}_2 + \text{H}_2\text{O}$, $\text{NO}_3 + \text{HC}$, $\text{N}_2\text{O}_5 + \text{H}_2\text{O}$ and $\text{N}_2\text{O}_5 + \text{Cl}^-$ pathway.